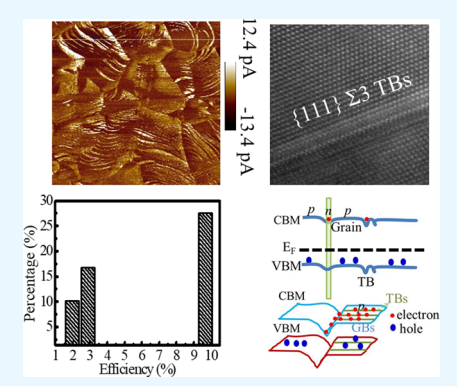
# Probing the Correlation of Twin Boundaries and Charge Transport of CdTe Solar Cells Using Electron Backscattering Diffraction and **Conductive Atomic Force Microscopy**

Hui Li,\*,†,‡,§® Paul Harrison,‡ Judy Wu,\*,‡ and Huijun Yao‡,

Supporting Information

ABSTRACT: The effect of grain boundaries (GBs) especially twin boundaries (TBs) on the performance of polycrystalline CdTe thin film (1–2  $\mu$ m in thickness) solar cells remains largely controversial. Understanding the GB's microstructure and physical property and their impact on the photovoltaic efficiency is critically important to the optimization of the solar cell performance. In this work, we present a systematic study of GBs in CdTe thin film solar cells of different efficiencies in the range of 1.97–9.68%, aiming to elucidate a quantitative correlation of GBs especially TBs with the solar cell charge transport by integrating several advanced approaches including electron backscattering diffraction, transmission electron microscopy, conductive atomic force microscopy, and scanning Kelvin probe force microscopy. Importantly, we have confirmed  $\{111\}$   $\Sigma 3$  TBs form in the PLD CdTe solar cells and are beneficial by providing an efficient channel for charge transport. The percentage of  $\{111\}$   $\Sigma 3$  TBs was found to be correlated quantitatively with the solar



cell power-conversion efficiency and a higher percentage led to a higher efficiency. In addition, a built-in field was observed between the random-angle GBs with respect to the grain interior, which may enhance exciton dissociation. This study provides a critical insight into the role of GBs in the polycrystalline CdTe thin film solar cells and is important to further improvement of their performance.

KEYWORDS: electron backscattering diffraction, photovoltaic, twin boundaries, conductive atomic force microscopy, thin film solar cells, CdTe solar cells, charge transport, twin boundaries enhanced current transport

m P olycrystalline thin (1–2  $\mu m$ ) and thick (up to 8–10  $\mu m$ ) film solar cells of cadmium telluride (CdTe), Cu-(In<sub>1-x</sub>Ga<sub>x</sub>)Se<sub>2</sub> (CIGS), and perovskite have been attracting intense attention both in basic research and industrial development due to their high efficiency and low cost. 1-8,21 The champion efficiencies for the CdTe, CIGS, and perovskite solar cells have reached to 22.1%, 22.6%, and 22.1%, respectively.<sup>5</sup> In these polycrystalline thin film solar cells, a large number of grain boundaries (GBs) are present. 1-8,21 It is well-known that GBs are rich in defects including dangling bonds, dislocations, and impurities. Therefore, most GBs are regarded as detrimental to solar cell performance since they may serve as charge carrier traps and recombination centers. 9-14 Understanding the GB's microstructure and physical property and their impact on the photovoltaic efficiency is therefore important to the optimization of the solar cell performance.

The GBs can be sensitively affected by the processing conditions. For example, in the CdTe thick film solar cells fabricated using a high-temperature method such as close space sublimation (CSS) and vapor transport deposition (VTD) with the substrate temperature higher than 500 °C for larger grain sizes and therefore a smaller concentration of GBs indeed exhibit much higher efficiency of >20% in laboratory cells and 18.6% on module cells. 15-20 Considerably lower efficiency was reported on CdTe thin film solar cells fabricated by a lowtemperature method with a substrate temperature lower than 500 °C such as pulsed laser deposition (PLD), radio frequency (RF) magnetic sputtering, electrodeposition, and screen-print deposition. 15-20 Consequently, the efficiency of PLD CdTe thin film solar cells is considerably lower than that of the CSS or VTD thick film counterparts. 15-20

A major difference between the lower-temperature PLD and higher-temperature CSS CdTe films is the much smaller grain size in the former as compared to that in the latter. This means that a significantly larger concentration of GBs is present in the PLD CdTe thin film solar cells. Understanding the GB effect is

Received: March 10, 2018 Accepted: July 2, 2018 Published: July 2, 2018



3646

<sup>†</sup>Institute of Electrical Engineering, Chinese Academy of Sciences, Beijing 100190, China

<sup>\*</sup>Department of Physics and Astronomy, University of Kansas, Lawrence, Kansas 66045, United States

<sup>§</sup>University of Chinese Academy of Sciences, Beijing 100049, China

Institute of Modern Physics, Chinese Academy of Sciences, Lanzhou 730000, China

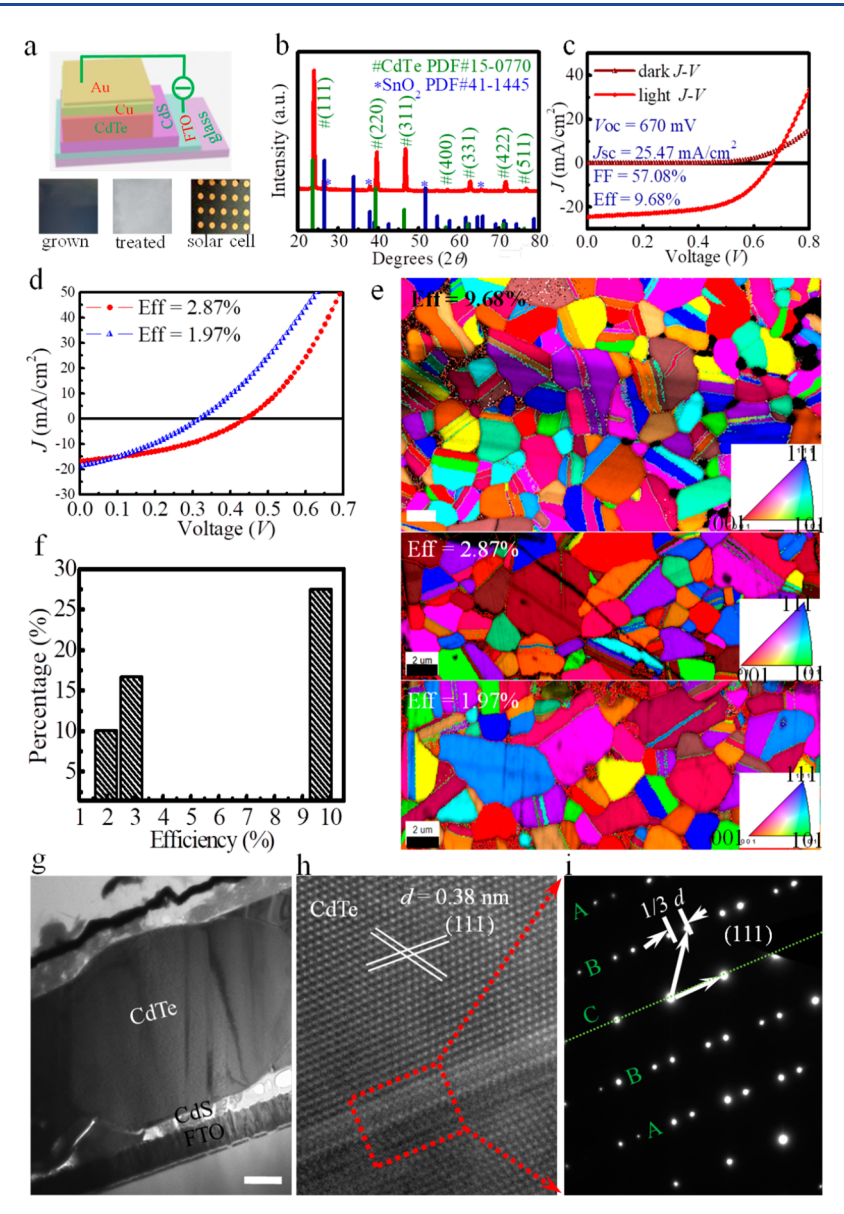


Figure 1. (a) Schematic illustration of a PLD CdTe solar cell and photographs of an as-grown CdTe, Cl-treated CdTe, and CdTe solar cell, respectively. (b) XRD  $\theta$ -2 $\theta$  spectrum of a Cl-treated CdTe thin film. (c) Dark and illuminated J-V curves for the CdTe solar cell with an efficiency of 9.68%. (d) Illuminated J-V curves for the CdTe solar cells with an efficiency of 1.97% and 2.87%, respectively. (e) EBSD images of the CdTe solar cells with efficiencies of 9.68%, 2.87%, and 1.97%, respectively. The scale bar is 2  $\mu$ m. The lower right side insets are the chaotic assortment of colors for the different crystallographic orientations of the corresponding EBSD image. (f) Relationship between percentage of {111}  $\Sigma$ 3 CSL TBs and efficiency of CdTe solar cell. (g) Bright-field TEM image of the cross-section of a CdTe solar cell. The scale bar is 0.5  $\mu$ m. (h) HRTEM image of a CdTe solar cell. (i) SAED pattern on dotted red rectangle in panel h. The stacking sequence is mirror-symmetric and the type of bonds remains the same, referring to a coherent {111}  $\Sigma$ 3 CSL TBs.

therefore important to further enhance the efficiency of the CdTe thin film solar cells. In fact, the CdTe solar cell currently takes the second largest market share after the silicon counterpart in the U.S. Especially, CdTe has a high absorption coefficient in exceeding  $10^5$  cm $^{-1}$  in the visible spectrum, which means that a CdTe thin film of  $\sim 1~\mu m$  in thickness can absorb  $\sim 90\%$  of photons with energy larger than its band gap of 1.45 eV. This makes CdTe thin film solar cells promising for commercial applications. The cost of CdTe solar cells has been reduced recently to \$0.40/Wp, making them competitive in large-scale commercialization.  $^{4-8}$ 

A few recent studies revealed that the GBs in CdTe polycrystalline films are not necessarily detrimental universally. <sup>22,27,33,47,48</sup> Instead, GBs especially twin boundaries (TBs)

assisted electrical current transport were reported. 21–27 However, a quantitative correlation between TBs and solar cell performance is lacking. Therefore, some questions are needed to further explore to clarify the formation and effect of GBs, especially TBs, on the performance of CdTe solar cells, which is also important to other polycrystalline thin films solar cells such as CIGS, perovskite for TBs' existence in these solar cells. Eirst of all, how does the synthesis method, such as CSS vs PLD or sputtering, affect the GB microstructures? Second, is the substrate temperature the most relevant parameter that determines the specific types of GBs formed in the polycrystalline CdTe films? Finally, how do the GBs especially TBs quantitatively impact with the performance of CdTe thin film solar cells? Answering these questions is important to

optimization of the CdTe solar cell performance, which is challenging since multiscale characterization is required to correlate the GB microstructures and electrical properties at a nanoscale with the charge transport at a device scale.

Motivated by this, we have carried out a quantitative study of the GBs in PLD CdTe thin film solar cells of different efficiencies of 1.97%, 2.87%, to 9.68% employing several advanced approaches including electron backscattering diffraction, transmission electron microscopy, conductive atomic force microscopy, and scanning Kelvin probe force microscopy. Interestingly, we have observed the  $\{111\}\ \Sigma 3$  TBs, for the first time to our knowledge, in the PLD CdTe thin film solar cells, similar to that in the CSS CdTe thick film solar cells. The percentage of the  $\{111\}$   $\Sigma 3$  TBs correlate closely with the processing conditions and are beneficial to exciton separation and charge transport. In particular, the solar cell efficiency increases monotonically with the percentage of  $\{111\}$   $\Sigma 3$  TBs. These results are therefore important to performance improvement of the CdTe polycrystalline thin film solar cells made by PLD and other low-temperature processes and other polycrystalline thin film solar cells.

#### ■ RESULTS AND DISCUSSION

The CdTe solar cell structure of TEC15 (glass/FTO)/CdS/ CdTe/Cu/Au is schematically illustrated in Figure 1a. The thicknesses of the CdS and CdTe are ~100 nm and ~1.5-2  $\mu$ m, respectively, measured using a Tencor P16 step profiler (Supporting Information Figure S1a) and confirmed by the cross-sectional SEM (Figure S1b). After the Cl treatment, the color of the CdTe surface changed from black into white color (Figure 1a), indicative of improvement in microstructure due to recrystallization of the CdTe and, hence, in the electrical performance of the CdTe solar cells. 24-27,29-31 In the case of the PLD CdTe thin film solar cells, the lateral grain size of Cltreated CdTe is in the range of 850 nm to  $\sim$ 4  $\mu$ m, much larger than that of the as-grown PLD CdTe with the grain size distributing in the range of 300-500 nm (Figure S1b-f). After the Cl treatment, no obvious cracks and voids were observable in the Cl-treated CdTe thin films, suggesting a low reverse leakage current in the obtained CdTe solar cells. X-ray diffraction (XRD)  $\theta$ -2 $\theta$  spectra further confirm high crystalline quality of the CdTe. The majority of XRD diffraction peaks in the Cl-treated (Figure 1b) and as-grown CdTe (Figure S2) can be indexed to the cubic CdTe with a reference ICDD card no. of 15-0770. The other diffraction peaks are indexed to SnO<sub>2</sub> with an ICDD card no. of 41-1445. However, after the Cl treatment, the preferred orientation changed from (220) to (111) (Figure S2 and Figure 1b). The full width at a half-maximum (fwhm) of the (111) peak is ~0.292° after the Cl treatment, in contrast to a slightly higher fwhm  $\sim 0.307^{\circ}$  of the (220) peak for the as-grown PLD CdTe films, further indicating higher crystalline quality.

Importantly, the surface of the Cl-treated CdTe surface is quite clean (Figure S1d,e) and Te-rich with a Cd and Te atomic ratio of 45.40:47.83 (Figure S3a,b), which may be due to the target Cd and Te atomic ratio of 49.98:50.02 (EDX, Figure S3c,d). CdTe after the Cl treatment has usually undergone the bromine treatment in order to form a Te-rich surface, which will introduce a wet chemical process and is not benign to the optoelectronic properties of CdTe. This is not suitable to large-scale solar cell production. Since the surface of the PLD CdTe is naturally Te-rich, no bromine treatment is needed in the PLD solar cell fabrication process, leading to a

simplified, low-cost process in our fabrication method. After the Cl treatment, an array of Cu (4 nm)/Au (50 nm) electrode was evaporated on the CdTe surface with a shadow mask. A 60 min postannealing was carried out at 170 °C in the Ar/O<sub>2</sub> atmosphere with an atomic ratio of 4:1 to facilitate Cu diffusion. The current density-voltage (I-V) curves were measured. Panels c and d of Figure 1 show the *I–V* curves of the three CdTe solar cells with efficiency of 9.68% (open circuit voltage  $(V_{oc})$  = 670 mV, short circuit current density  $(J_{sc}) = 25.47 \text{ mA/cm}^2$ , fill factor (FF) = 57.08%), 2.87% ( $V_{oc}$  = 439 mV,  $J_{sc}$  = 16.76 mA/cm<sup>2</sup>, FF = 38.96%), and 1.97% ( $V_{oc}$  = 318 mV,  $J_{sc} = 18.73$  mA/cm<sup>2</sup>, FF = 33.07%). To understand the correlation between the efficiency and microstructure, electron backscattering diffraction (EBSD) was conducted on the area cut by a FIB (Figure S4a) in the PLD CdTe solar cells with different efficiencies to quantify the GBs. The results for the three samples of different efficiencies of 9.68%, 2.87%, and 1.97% are shown in Figure 1e and Figures S4-S7. On the 9.68%-efficient sample, the EBSD revealed that the majority of GBs are large angle GBs have rotation angles in the range of 15-180°. Importantly, among the large-angle GBs, 57.3%, 46.0%, and 40.5% are coherent, or coincidence site lattice (CSL), while 40.9%, 52.8%, and 57.8% are incoherent with random angles in the CdTe solar cells with efficiencies of 9.68%, 2.87%, and 1.97%, respectively (Figures S5-S7). This means incoherent large-angle GBs are unfavorable.<sup>31</sup> Among the CSL TBs, most of them are misoriented at  $60^{\circ}$  (111) (Figure S5), indicating most of the CSL TBs are prevalent  $\Sigma$ 3  $\{111\}$  TBs in CdTe films.  $^{26,27,31}$  Besides the  $\{111\}$   $\Sigma 3$  CSL coherent TBs, some incoherent TBs, i.e., boundaries with twin misorientation but a boundary plane different from the coherent {111} mirror plane was also observed (Figures S5-S7). These incoherent TBs were found to be electrically active due to presence of massive defects, resulting in detrimental charge recombination.<sup>30</sup> Transmission electron microscopy (TEM) was further conducted to characterize the CdTe solar cells. It is seen from the bright-field TEM image (Figure 1g) and high-resolution TEM (HRTEM) images (Figure 1h) that the stacking sequence is mirror-symmetric (ABClCBA), which is referred to as a coherent  $\Sigma$ 3 CSL TBs.<sup>32</sup> The calculated d value is 0.38 nm, consistent with the  $\{111\}$  space of CdTe (d =0.37 nm; Figure 1i), which demonstrates that the CSL boundaries are indeed  $\Sigma$ 3 CSL {111} TBs. To our knowledge, this is the first observation of  $\{111\}$   $\Sigma 3$  CSL TBs in the PLD CdTe thin films, while TBs are popular in CSS CdTe.<sup>26</sup> The formation of  $\{111\}$   $\Sigma 3$  CSL TBs is due to its low formation energy of about 9.0  $\pm$  1 mJ/m<sup>2.27</sup> As shown in the EBSD image (Figure 1e and Figure S4b), the fraction of the  $\Sigma$ 3 CSL {111} TBs is higher at the CdTe film thickness closer to the CdTe/CdS pn junction, which is consistent with a prior report.<sup>31</sup> On the 1.97%, 2.87%, and 9.68% efficiency samples, the  $\{111\}$   $\Sigma 3$  CSL TBs are 10.09%, 16.69%, to 27.55%, respectively, out of the total amount of the large-angle GBs (Figures 1e,f and S5-S7). This indicates that the percentage of  $\{111\}$   $\Sigma 3$  CSL TBs increases with the efficiency (Figure 1f), implying the beneficial effect of  $\{111\}$   $\Sigma 3$  CSL TBs on the performance of CdTe solar cells. The percentages of incoherence with random angles on the 1.97%, 2.87%, and 9.68% efficiency samples are 40.9%, 52.8%, and 57.8%, respectively, as shown in Figure 1e,f and Figures S5-S7. In addition, the direction of {111} boundaries changes from [100] in CdTe with an efficiency of 9.68% to [001] in CdTe with an efficiency of 2.87% (Figures S5 and S6). Finally, in

CdTe with an efficiency of 1.97%, the [001] direction of {111} boundaries becomes quite weak (Figure S7). The decreasing solar cell efficiency with the fraction of the [100] growth direction of the {111} boundaries suggests that the [100] growth direction is favorable for the  $\Sigma$ 3 CSL TBs to provide beneficial effect to charge transport.

The beneficial effect of GBs especially CSL TBs in the CdTe solar cell is further confirmed by the conductive—atomic force microscopy (C-AFM) measurement using a Pt/Ir-coated conductive probe in contact mode with a 0 V DC voltage applied to the tip.<sup>27</sup> The result for the CdTe solar cell with an efficiency of 9.68% is shown in Figure 2. It is seen from the

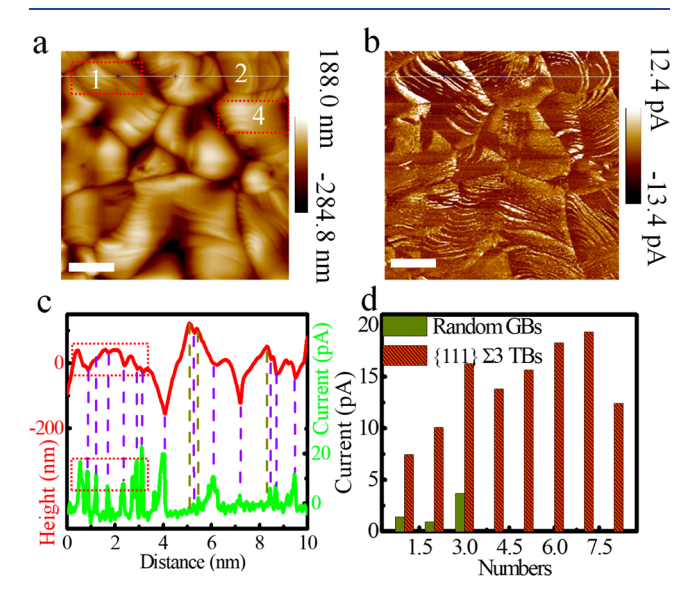
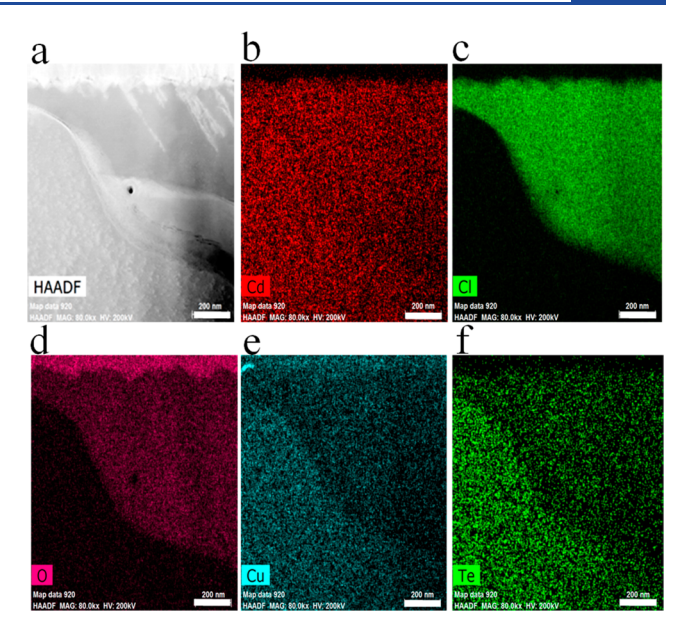


Figure 2. (a) AFM image of a Cl-treated CdTe film. (b) Conductive AFM (C-AFM) current map with DC tip voltage (TV) of 0 V. (c) AFM line scan (red) and C-AFM line scan (green) on a Cl-treated CdTe, showing GBs especially TB-enhanced current transport. (d) Current value at the {111}  $\Sigma$ 3 CSL TBs and random GBs of Cl-treated CdTe. The numbers in the horizontal axis present the number of GBs and TBs along the cross-section line shown in panels a and b. The scale bars in panels a and b are 5  $\mu$ m.

cross-section lines of the CdTe height and C-AFM images (Figure 2a–c) that the current induced by the 633 nm laser of the scanning probe microscopy (SPM) value is significantly larger at the GBs as compared with that on the grain interiors (GIs). In addition, the current value at the TBs of the CdTe polycrystalline thin film is much larger than that at the GBs of random GB angles (Figure 2d). Therefore, in CdTe solar cells, GBs, especially the {111}  $\Sigma$ 3 CSL TBs, are electrically beneficial to enhanced charge transport. This observation is important to further improvement of the PLD CdTe thin film solar cell performance.<sup>30</sup> Furthermore, the  $\Sigma$ 3 CSL TBs with [100] growth direction indeed has much better effect on the microcurrent transport as illustrated in the C-AFM image in Figure 2b, which is consistent with the reported results.<sup>27</sup>

To explain the reason for the current difference between the GBs, including TBs and GIs, we conducted TEM analysis and the results are depicted in Figure 3 on GBs of random angles and in Figure 4 on  $\{111\}$   $\Sigma 3$  CSL TBs. We also have measured the elemental distribution across random GBs and  $\{111\}$   $\Sigma 3$  CSL TBs at both grains (Figure 3) and tilted edges (Figure S8). Similar properties of the Cl were observed (Figure S8). Interestingly, the neighboring two grains across the former



**Figure 3.** (a) Bright-field TEM image of a random GB in a CdTe film after Cl treatment. (b) Cd, (c) Cl, (d) O, (e) Cu, and (f) Te element maps of the area shown in panel a. The scale bar is 200 nm.

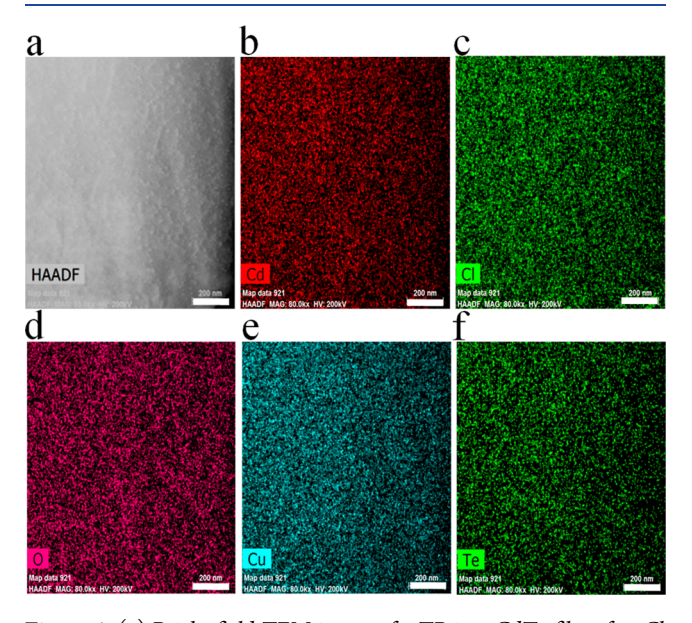


**Figure 4.** (a) Bright-field TEM image of a TB in a CdTe film after Cl treatment. (b) Cd, (c) Cl, (d) O, (e) Cu, and (f) Te element maps over the area shown in panel a. The scale bar is 200 nm.

have different elements compositions. One of the grains is Cl, O-rich CdTe and the other is Cu, Te-rich CdTe (Figure 3). The CdTe grain with Cl, O-rich commonly shows n-type while the CdTe grain with Cu, Te-rich commonly shows p-type,  $^{34}$  leading to formation of a local p—n junction between the neighboring CdTe grains. The electrical field is the biggest in proximity of the GBs, leading to the photogenerated electron following to the proximity of the GBs. This is proved by the SKPFM measurement, as shown in Figure 5. When conducting SKPFM measurement, the distance between the CdTe surface and tip was maintained at 50 nm. In addition, the oscillating electrostatic forces were minimized by applying a compensating  $V_{\rm DC}$  to the tip. From the SKPFM mapping and the corresponding cross-section lines (Figure 5), the contact

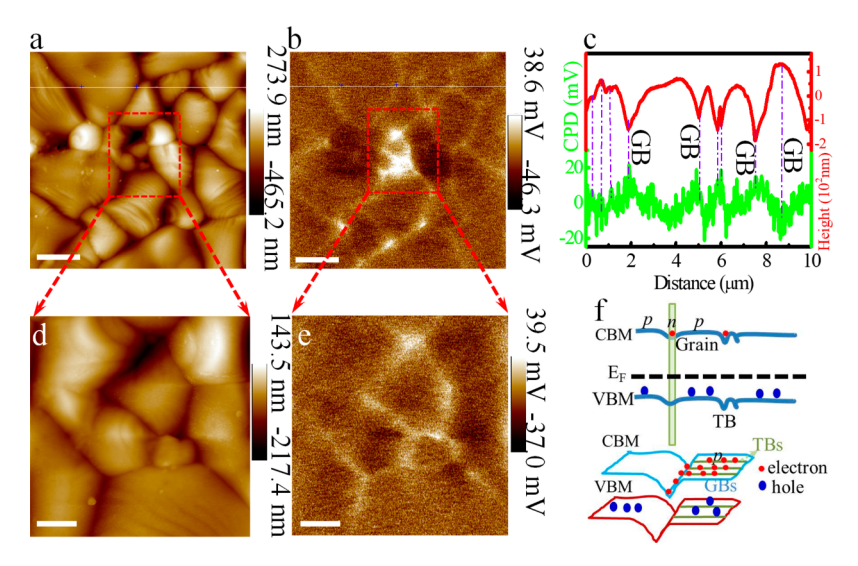


Figure 5. (a) AFM image of a Cl-treated PLD CdTe film and (b) a corresponding SKPFM image of the same sample in panel a. (c) AFM line scan (red) and SKPFM line scan (green) of the Cl-treated CdTe. Magnified AFM image (d) and SKPFM image (e) of the Cl-treated CdTe in panel a. (f) Schematic description of the beneficial effect of GBs, especially TBs, in the CdTe solar cell. The CBM and the VBM are the conduction band minima and valence band maxima, respectively.

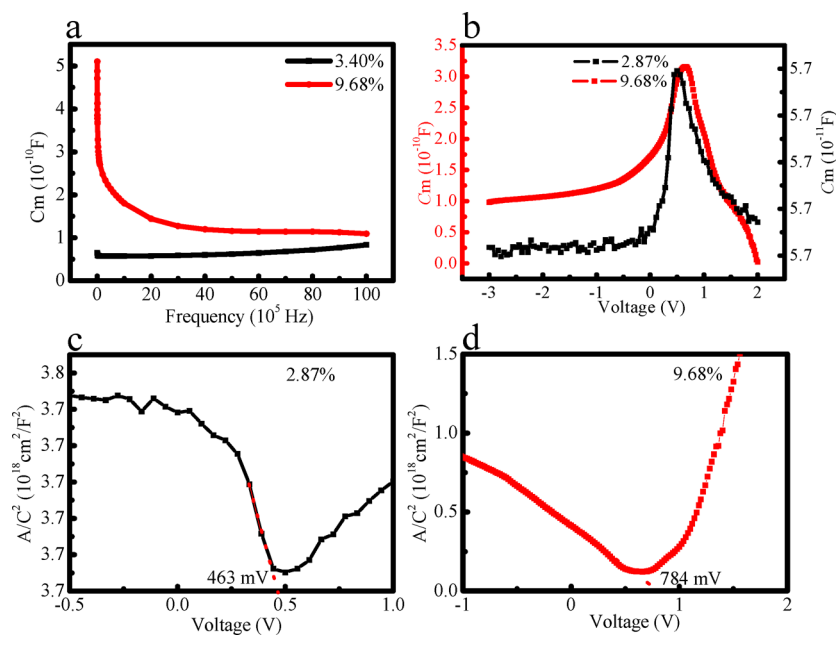


Figure 6. (a) C-f curves and (b) C-V curves at 800 kHz.for the CdTe solar cells with 9.68% and 2.87% efficiency, respectively.  $C^{-2}-V$  curve at frequencies of 800 kHz for the CdTe solar cell with (c) a 2.87% efficiency, giving an internal electrical field  $(V_{bi})$  value of 0.463 V, and (d) a 9.68% efficiency, giving a  $V_{bi}$  value of 0.784 V.

potential difference (CPD) is observed between the GIs and GBs (Figure 5). Thus, the CPD induces a local electric field, which facilitates separation of electrons and holes during light absorption in the lateral direction of the CdTe polycrystalline thin film. The CPD can be determined from  $V_{\rm CPD} = -V_{\rm DC} = e(W_{\rm sample} - W_{\rm tip})$ , where W is the work function and e is the electron charge. Thus, the work function is the smallest at the GBs, leading to the photogenerated electron following to the proximity of the GBs. However, no element difference is found in the CdTe grains with TBs (Figure 4). In addition, the potential difference between TBs and GIs is quite small as expected (Figure 5). The TBs' enhanced current transport is therefore most probably due to its lower resistivity than that of the GIs. The GIs is a local electric field, which is observed and the control of the GIs. The TBs' enhanced current transport is therefore most probably due to its lower resistivity than that of the GIs.

Capacitance—voltage (C-V) characterization was conducted in the frequency range of 1 kHz to 6 MHz in the dark, and the result is illustrated in Figure S9a. The measured capacitance  $(C_{\rm m})$  shows no change when the frequency is between 1 and 10 kHz. Compared with the  $C_{\rm m}$  values measured at the frequency range of 1 kHz to 6 MHz, the  $C_{\rm m}$  values become smaller at the frequency range of 50–800 kHz. The  $C_{\rm m}$  values of the CdTe solar cells with efficiencies of 2.87% and 9.68% further become smaller when the frequency is higher than 800 kHz (Figure 6a). The measured  $C_{\rm m}$  mainly consist of junction capacitance  $(C_{\rm j})$  and trap capacitance  $(C_{\rm t})$ .  $C_{\rm j}$  is frequency independent while  $C_{\rm t}$  changes with frequency because traps generally only follow the external AC signal at low and intermediate frequencies.<sup>36</sup> The decrease of  $C_{\rm m}$  at higher

frequencies (Figure S9a,c) indicates that the  $C_{\rm m}$  consists of  $C_{\rm i}$ and  $C_t$  at low and intermediate frequency while the  $C_m$  is dominated by the  $C_j$  at higher frequency.<sup>36</sup> Thus, we can calculate the carrier density in the CdTe solar cells with efficiencies of 2.87% and 9.68% based on the  $C_m-V$  curves measured at higher frequencies of 800 kHz (Figure 6b) according to the following eq 1:<sup>37</sup>

$$N(a) = \frac{2}{qE_{\rm s}[d(C^{-2})/dV]}$$
 (1)

where N(a) is the carrier density  $(1/cm^3)$ , q is the electron charge (1.60219  $\times$  10<sup>-19</sup> C),  $E_s$  is the semiconductor permittivity (1.034  $\times$  10<sup>-12</sup> F/cm for CdTe), C is the measured capacitance (F), and V is the applied DC voltage (V). The value of the  $d(C^{-2})/dV$  can be obtained from the slope of the curve of  $C^{-2}-V$ , as shown in Figure 6c,d. The calculated carrier densities for the CdTe solar cell with efficiencies of 2.87% and 9.68% are about  $9.8 \times 10^{12}$  and  $2.4 \times$ 10<sup>13</sup> cm<sup>-3</sup>, respectively, smaller than that of CSS CdTe.<sup>38</sup> The low hole density results in a low  $V_{\rm oc}$  value of 670 mV, which may be a critical limitation of the CdTe solar cells performance.<sup>39</sup> Thus, it is seen that the carrier density increases with the efficiency, corresponding to increasing with the percentage of  $\{111\}$   $\Sigma 3$  TBs. This may be due to the enhanced carrier collection ability of  $\{111\}\ \Sigma 3$  TBs, leading to more carrier reach to the electrodes. The built-in voltage  $(V_{\rm bi})$ of the cell junction was derived from the intersection of the 1/  $C^2$  curve and the horizontal axis (Figure S9b), which yielded a  $V_{\rm bi} \sim 0.463~{
m V}$  (CdTe solar cell with efficiency of 2.87%) and  $V_{\rm bi} \sim 0.784 \text{ V}$  (CdTe solar cell with efficiency of 9.68%), as shown in Figure 6c,d.

Therefore, by increasing the percentage of  $\{111\}$   $\Sigma 3$  TBs, an efficiency of 9.68% has been achieved, which is ~45% improvement over the best previously reported on the CdTe solar cells fabricated by the PLD method. This solar cell was further characterized. The dark and illumination J-V curves of CdTe solar cell with an efficiency of 9.68% (Figure 1c) are crossed above the  $V_{oc}$  indicating an electron barrier in the conduction band which is possibly due to a high density of acceptors in the CdTe absorber, near the p-n interface region. Upon illumination, the absorber acceptors are filled with holes which are photogenerated in the buffer layers. As a result, the acceptor charge is reduced and so is the electron barrier, resulting in the crossed point above the  $V_{\rm oc}$ . It has been welldocumented that a mixed CdS<sub>x</sub>Te<sub>1-x</sub> crystal is typically formed at the CdTe/CdS interface due to the chemical interdiffusion during the fabrication process. The formation of a  $CdS_rTe_{1-r}$ interfacial layer is thought to be responsible for decreasing structural defects due to the lattice mismatch (about 10%) between CdS and CdTe, leading to a lower defect density at this critical part of the device.  $^{39,40}$  The formation of CdS<sub>1-x</sub>Te<sub>x</sub> alloy can be determined from the external quantum efficiency (EQE) curve. As shown in Figure S10, the absence of a distinct cutoff at 510 nm in the response of the CdTe solar cells indicates the formation of a  $CdS_{1-x}Te_x$  alloy due to the Te diffusion into the CdS films. 41 The EQE curve further shows that the absorption loss in the CdTe solar cell is mainly due to the absorption loss of glass and CdS. 42 The result indicates that a considerable  $J_{sc}$  enhancement is possible in this case by employing a thinner CdS window and using a different glass. The band gap of CdTe determined from the EQE and differential EQE curve is 1.47 eV (Figure S10), which is

consistent with that of CdTe fabricated by another deposition method such as CSS method.<sup>36</sup>

Panels a-d of Figure S11 show the relationship of Eff,  $V_{OC}$ , FF, and  $I_{sc}$  between light intensity for the CdTe solar cell. As shown in Figure S11, the Eff values increase with the decrease of the light intensity in the range of 100 to 20 mW/cm<sup>2</sup>, indicating good weak light effect of the PLD CdTe solar cell. It is well-known that some parameters such as the ideality factor (A) can be deduced from the following eqs 2-5:<sup>37</sup>

$$J = J_0 \left\{ \exp\left(\frac{q(V - R_s J)}{AKT}\right) - 1 \right\} - J_L + G(V - JR_s)$$
 (2)

where T is the temperature, K is the Boltzmann constant,  $I_L$  is the photogenerated current density, A is the ideality factor,  $R_s$ is the series resistance, G is the parallel conductance, and  $J_0$  is the diode reverse saturation current density.

$$g(V) = \frac{\mathrm{d}J}{\mathrm{d}V} = J_0 \frac{q - R_s \frac{\mathrm{d}J}{\mathrm{d}V}}{AKT} \exp\left[\frac{q(V - JR_s)}{AKT}\right] + G \tag{3}$$

$$\left(\frac{\mathrm{d}J}{\mathrm{d}V}\right)_{V\leq 0} = G\tag{4}$$

$$\ln(J + J_{\rm L} - GV) = \ln J_0 + \frac{q(V - JR_{\rm s})}{AKT}$$
(5)

Thus, G is about 5 and 0.01 mS cm<sup>-2</sup> obtained from the dependence of dI/dV on the voltage curve (Figure S12).<sup>38</sup> The value of A is about 1.4 obtained from the dependence of dV/dJon the  $(J + J_{sc})^{-1}$  curve (Figure S12), showing that the recombination is dominated by the space-charge region. 43,44 The second recombination is the interface recombination, which is maybe coexisting with the recombination in the spacecharge region.

## **CONCLUSIONS**

In conclusion, a systematic study of the GBs in polycrystalline CdTe thin film solar cells made with low-temperature PLD method has been carried out to elucidate the quantitative correlation between microstructure and electric properties of the GBs with the solar cell performance. Several important insights have been obtained. First, a high concentration of the  $\{111\}$  CSL  $\Sigma 3$  TBs was observed in the PLD CdTe thin films. These TBs are significantly more conductive than the GBs of random GB angles and are therefore beneficial to the charge carrier transport. Second, the percentage of  $\{111\}$   $\Sigma 3$  TBs was found to correlate quantitatively with the solar cell performance. Specifically, the efficiency of CdTe solar cells increases monotonically with the percentage of  $\{111\}$   $\Sigma 3$  TBs, further confirming the beneficial effect of the  $\{111\}$   $\Sigma 3$  TBs on the performance of CdTe solar cells. A power conversion efficiency up to 9.68% has been obtained on PLD CdTe thin film solar cells with higher  $\{111\}$   $\Sigma 3$  TB concentration of 27.55%, in contrast to the lower  $\{111\}$   $\Sigma 3$  TB of 10.09% in a cell of 1.97% efficiency. The carrier density is also increased with the percentage of  $\{111\}$   $\Sigma 3$  TBs due to the enhanced carrier transport ability with the  $\{111\}$   $\Sigma 3$  TBs percentage enhancement. Finally, a local electrical field between the different GIs and the random GBs may provide a built-in electric field for exciton separation and charge transfer. This result therefore suggests GBs, especially  $\{111\}$   $\Sigma 3$  TBs, can be beneficial in PLD CdTe thin film solar cells and optimization of the GBs is important to further improve the solar cell performance.

#### METHODS

**Experiments.** TEC15 substrates from Pilkington Inc. were ultrasonicated for 10 min each in acetone and isopropyl alcohol, respectively, before being mounted into the PLD system for in situ growth of CdS and CdTe polycrystalline thin films. The details of the PLD procedure have been published elsewhere.  $^{45,46}$  After the PLD growth, the CdTe/CdS samples underwent Cl treatment in a tube furnace under the Ar/O $_2$  atmosphere with ratios of 0:1–1:0 at 390–410 °C for about 40–60 min. To conduct the Cl treatment, the CdCl $_2$  and methanol mixed solution was dip-coated onto a glass slide and placed on a heating stage until the methanol was completely vaporized. In the processing window of this work, the best crystalline quality of the PLD CdTe polycrystalline thin film was observed using the Cl treatment at 400 °C for 60 min under the 4:1 Ar/O $_2$  atmosphere.

XRD was carried out using a PANalytical X'Pert PRO diffractometer equipped with Cu K $\alpha$  radiation ( $\lambda$  = 1.54050 Å). For EBSD sample preparation, a FEI Helio Nano Lab Nova200 dual beam system (FEI Co., Hillsboro, OR, USA), equipped with both electron and focused Ga+ ion beams (FIBs), was used to cut a flat analysis plane at 1.5° with respect to the film surface for EBSD. A mill box of 30  $\mu$ m × 20  $\mu$ m × 1.5  $\mu$ m was positioned on the film surfaces and milled at 30 kV beam energy and 1 nA of beam current for about 10 min. The EBSD was conducted in a PHI 710 Auger electron spectrometer (AES) equipped with an EBSD detector. The FIB cut SEM image and the corresponding EBSD images are shown in Figure S4 and Figure 1e, respectively. Specifically, as shown in Figure S4b, the EBSD study can be carried out through the CdTe film continuously from the bottom near CdS to the surface near the back-contact. All C-AFM and SKPFM analyses were performed directly on the CdTe surface instead of the area cut by FIB using scanning probe microscopy (ICON2-SYS, Bruker Nano Inc., Ewing, NJ, USA). This is because the Ga+ ion beam altered the surface layer (typically 1-2 nm in thickness) of the cut area for EBSD. The modified layer Ga doping acted like a tunnel barrier to prevent electron transport in C-AFM measurement. J-V curves were recorded using a Keithley 2636A source meter under simulated solar light illumination (1 sun, 100 mW cm<sup>-2</sup>) generated by a Newport 96000 solar simulator equipped with an AM 1.5G filter. The light intensity was calibrated with a Newport 91150 V reference cell before each measurement. I-V characterization of the synthesized cells was conducted under standard test condition. A Newport Oriel 91159A solar simulator (Newport Corp., CA, USA) was used to generate an AM 1.5 irradiance of 100 mW cm<sup>-2</sup>. The surface topography and composition analyses of the samples were conducted on a Zeiss  $\sigma$ -type scanning electron microscope (Carl Zeiss Corp, Oberkochen, Germany), which was also used for EDX analysis. The C-V data were collected using 4200-SCS Keithley, Tektronix. The transmission electron microscope (TEM) characterizations were performed on Tecnai G2 F20 S-Twin (the spot and line resolution are 0.24 and 0.102 nm, respectively) with a voltage of 200 kV. For preparing the sample for TEM characterization, the sample was mechanically thinned and then thinned using a Gatan691 precision ion polishing

## ■ ASSOCIATED CONTENT

#### Supporting Information

The Supporting Information is available free of charge on the ACS Publications website at DOI: 10.1021/acsaem.8b00382.

Figures showing various images of samples and characteristic distributions, XRD patterns, EDX spectra, EBSD image and results, pole figures and intensities, misorientation angle distribution, bright-field TEM images, C-V,  $C^2-V$ , and EQE curves, light intensity dependencies, and dJ/dV and dV/dJ plots (PDF)

#### AUTHOR INFORMATION

### **Corresponding Authors**

\*(H.L.) E-mail: lihui@mail.iee.ac.cn.

\*(J.W.) E-mail: jwu@ku.edu.

ORCID ®

Hui Li: 0000-0001-8883-8518 Huijun Yao: 0000-0002-9684-8254

#### Notes

The authors declare no competing financial interest.

#### ACKNOWLEDGMENTS

This work was supported by the National Natural Science Foundation of China (Grant Nos. 51472239 and 11575261) and the Youth Innovation Promotion Association, CAS (Grant No. 2014122). J.W. acknowledges support in part by USARO Contract No. W911NF-16-1-0029 and USNSF Contract Nos. NSF-DMR-1337737 and NSF-DMR-1508494.

#### REFERENCES

- (1) Hsu, C. H.; Ho, W. H.; Wei, S. Y.; Lai, C. H. Over 14% Efficiency of Directly Sputtered Cu(In,Ga)Se<sub>2</sub> Absorbers without Post Selenization by Post-Treatment of Alkali Metals. *Adv. Energy Mater.* **2017**, *7*, 1602571.
- (2) Green, M. A.; Ho-Baillie, A.; Snaith, H. J. The Emergence of Perovskite Solar Cells. *Nat. Photonics* **2014**, *8*, 506–514.
- (3) Green, M. A.; Bremner, S. P. Energy Conversion Approaches and Materials for High-Efficiency Photovoltaics. *Nat. Mater.* **2017**, *16*, 23–26.
- (4) Barnard, E. S.; Ursprung, B.; Colegrove, E.; Moutinho, H. R.; Borys, N. J.; Hardin, B. E.; Peters, C. H.; Metzger, W. K.; Schuck, P. J. 3D Lifetime Tomography Reveals How CdCl<sub>2</sub> Improves Recombination Throughout CdTe Solar Cells. *Adv. Mater.* **2017**, *29*, 1603801.
- (5) Green, M. A.; Hishikawa, Y.; Warta, W.; Dunlop, E. D.; Levi, D. H.; Hohl-Ebinger, J.; Ho-Baillie, A. W. Y. Solar Cell Efficiency Tables (Version 50). *Prog. Photovoltaics* **2017**, *25*, 668–676.
- (6) Kumar, S. G.; Rao, K. S. R. K. Physics and Chemistry of CdTe/CdS Thin Film Heterojunction Photovoltaic Devices: Fundamental and Critical Aspects. *Energy Environ. Sci.* **2014**, *7*, 45–102.
- (7) Jasieniak, J.; MacDonald, B. I.; Watkins, S. E.; Mulvaney, P. Solution-Processed Sintered Nanocrystal Solar Cells via Layer-by-Layer Assembly. *Nano Lett.* **2011**, *11*, 2856–2864.
- (8) Kranz, L.; Gretener, C.; Perrenoud, J.; Schmitt, R.; Pianezzi, F.; La Mattina, F.; Blösch, P.; Cheah, E.; Chirila, A.; Fella, C. M.; Hagendorfer, H.; Jäger, T.; Nishiwaki, S.; Uhl, A. R.; Buecheler, S.; Tiwari, A. N. Doping of Polycrystalline CdTe for High-Efficiency Solar Cells on Flexible Metal Foil. *Nat. Commun.* **2013**, *4*, 2306.
- (9) Kanevce, A.; Reese, M. O.; Barnes, T. M.; Jensen, S. A.; Metzger, W. K. The Roles of Carrier Concentration and Interface, Bulk, and Grain-Boundary Recombination for 25% Efficient CdTe Solar Cells. *J. Appl. Phys.* **2017**, 121, 214506.
- (10) Sherkar, T. S.; Momblona, C.; Gil-Escrig, L.; Avila, J.; Sessolo, M.; Bolink, H. J.; Koster, L. J. A. Recombination in Perovskite Solar Cells: Significance of Grain Boundaries, Interface Traps, and Defect Ions. ACS Energy Lett. 2017, 2, 1214–1222.
- (11) Das, S. K.; Morris, G. C. Influence of Growth and Microstructure of Electrodeposited Cadmium Telluride Films on the Properties of n CdS/pCdTe Thinfilm Solar Cells. *J. Appl. Phys.* **1992**, 72, 4940–4945.
- (12) Major, J. D.; Proskuryakov, Y. Y.; Durose, K.; Zoppi, G.; Forbes, I. Control of Grain Size in Sublimation-Grown CdTe, and the Improvement in Performance of Devices with Systematically Increased Grain Size. Sol. Energy Mater. Sol. Cells 2010, 94, 1107—1112
- (13) Mendis, B. G.; Bowen, L.; Jiang, Q. Z. A Contactless Method for Measuring the Recombination Velocity of an Individual Grain

- Boundary in Thin-Film Photovoltaics. Appl. Phys. Lett. 2010, 97, 092112.
- (14) Moseley, J.; Al-Jassim, M. M.; Moutinho, H. R.; Guthrey, H. L.; Metzger, W. K.; Ahrenkiel, R. K. Explanation of Red Spectral Shifts at CdTe Grain Boundaries. *Appl. Phys. Lett.* **2013**, *103*, 233103.
- (15) Wu, X. Z. High-Efficiency Polycrystalline CdTe Thin-Film Solar Cells. Sol. Energy 2004, 77, 803–814.
- (16) Li, H.; Liu, X.; Yang, B.; Wang, P. Influence of Substrate Bias and Post-Deposition Cl Treatment on CdTe Film Grown by RF Magnetron Sputtering for Solar Cells. RSC Adv. 2014, 4, 5046–5054.
- (17) Kestner, J. M.; McElvain, S.; Kelly, S.; Ohno, T. R.; Woods, L. M.; Wolden, C. A. An Experimental and Modeling Analysis of Vapor Transport Deposition of Cadmium Telluride. *Sol. Energy Mater. Sol. Cells* **2004**, *83*, 55–65.
- (18) Li, B.; Liu, J. W.; Xu, G. W.; Lu, R. T.; Feng, L. H.; Wu, J. Development of Pulsed Laser Deposition for CdS/CdTe Thin Film Solar Cells. *Appl. Phys. Lett.* **2012**, *101*, 153903.
- (19) Liu, B.; Luo, R.; Li, B.; Zhang, J. Q.; Li, W.; Wu, L. L.; Feng, L. H.; Wu, J. D. Effects of Deposition Temperature and CdCl<sub>2</sub> Annealing on the CdS Thin Films Prepared by Pulsed Laser Deposition. *J. Alloys Compd.* **2016**, *654*, 333–339.
- (20) Lowndes, D. H.; Geohegan, D. B.; Puretzky, A. A.; Norton, D. P.; Rouleau, C. M. Synthesis of Novel Thin-Film Materials by Pulsed Laser Deposition. *Science* **1996**, 273, 898–903.
- (21) Chirila, A.; Buecheler, S.; Pianezzi, F.; Bloesch, P.; Gretener, C.; Uhl, A. R.; Fella, C.; Kranz, L.; Perrenoud, J.; Seyrling, S.; Verma, R.; Nishiwaki, S.; Romanyuk, Y. E.; Bilger, G.; Tiwari, A. N. Highly Efficient Cu(In,Ga)Se<sub>2</sub> Solar Cells grown on Flexible Polymer Films. *Nat. Mater.* **2011**, *10*, 857–861.
- (22) Luria, J.; Kutes, Y.; Moore, A.; Zhang, L.; Stach, E. A.; Huey, B. D. Charge Transport in CdTe Solar Cells Revealed by Conductive Tomographic Atomic Force Microscopy. *Nature Energy* **2016**, *1*, 16150.
- (23) Visoly-Fisher, I.; Cohen, S. R.; Ruzin, A.; Cahen, D. How Polycrystalline Devices Can Outperform Single-Crystal Ones: Thin Film CdTe/CdS Solar Cells. *Adv. Mater.* **2004**, *16*, 879–883.
- (24) Tuteja, M.; Koirala, P.; Palekis, V.; MacLaren, S.; Ferekides, C. S.; Collins, R. W.; Rockett, A. A. Direct Observation of CdCl<sub>2</sub> Treatment Induced Grain Boundary Carrier Depletion in CdTe Solar Cells Using Scanning Probe Microwave Reflectivity Based Capacitance Measurements. J. Phys. Chem. C 2016, 120, 7020–7024.
- (25) Li, W. J.; Ma, Y. P.; Yang, S. H.; Gong, J. B.; Zhang, S. B.; Xiao, X. D. Nanoscopic Study of the Compositions, Structures, and Electronic Properties of Grain Boundaries in Cu(InGa)Se<sub>2</sub> Photovoltaic Thin Films. *Nano Energy* **2017**, *33*, 157–167.
- (26) Korevaar, B. A.; Cournoyer, J. R.; Sulima, O.; Yakimov, A.; Johnson, J. N. Role of Oxygen During CdTe Growth for CdTe Photovoltaic Devices. *Prog. Photovoltaics* **2014**, *22*, 1040–1049.
- (27) Li, H.; Liu, X.; Lin, Y.; Yang, B.; Du, Z. Enhanced Electrical Properties at Boundaries Including Twin Bboundaries of Polycrystal-line CdTe Thin-Film Solar Cells. *Phys. Chem. Chem. Phys.* **2015**, *17*, 11150–11155.
- (28) Schöppe, P.; Schönherr, S.; Würz, R.; Wisniewski, W.; Martínez-Criado, G.; Ritzer, M.; Ritter, K.; Ronning, C.; Schnohr, C. S. Rubidium Segregation at Random Grain Boundaries in Cu(In,Ga)Se<sub>2</sub> Absorbers. *Nano Energy* **2017**, *42*, 307–313.
- (29) Major, J. D.; Treharne, R. E.; Phillips, L. J.; Durose, K. A Low-Cost Non-Toxic Post-Growth Activation step for CdTe Solar Cells. *Nature* **2014**, *511*, 334–337.
- (30) Stechmann, G.; Zaefferer, S.; Schwarz, T.; Konijnenberg, P.; Raabe, D.; Gretener, C.; Kranz, L.; Perrenoud, J.; Buecheler, S.; Nath Tiwari, A. A Correlative Investigation of Grain Boundary Crystallography and Electronic Properties in CdTe Thin Film Solar Cells. *Sol. Energy Mater. Sol. Cells* **2017**, *166*, 108–120.
- (31) Stechmann, G.; Zaefferer, S.; Konijnenberg, P.; Raabe, D.; Gretener, C.; Kranz, L.; Perrenoud, J.; Buecheler, S.; Tiwari, A. N. 3-Dimensional Microstructural Characterization of CdTe Absorber Layers From CdTe/CdS Thin Film Solar Cells. *Sol. Energy Mater. Sol. Cells* **2016**, *151*, 66–80.

- (32) Li, C.; Poplawsky, J.; Yan, Y.; Pennycook, J. Understanding Individual Defects in CdTe Thin-Film Solar Cells via STEM: From Atomic Structure to Electrical Activity. *Mater. Sci. Semicond. Process.* **2017**, *65*, 64–76.
- (33) Li, C.; Wu, Y.; Poplawsky, J.; Pennycook, T. J.; Paudel, N.; Yin, W.; Haigh, S. J.; Oxley, M. P.; Lupini, A. R.; Al-Jassim, M.; Pennycook, S. J.; Yan, Y. Grain-Boundary-Enhanced Carrier Collection in CdTe Solar Cells. *Phys. Rev. Lett.* **2014**, *112*, 156103.
- (34) Lindström, A.; Klintenberg, M.; Sanyal, B.; Mirbt, S. Cl-Doping of Te-Rich CdTe: Complex Formation, Self-Compensation and Self-Purification From First Principles. *AIP Adv.* **2015**, *5*, 087101.
- (35) Lu, L.; Shen, Y.; Chen, X.; Qian, L.; Lu, K. Ultrahigh Strength and High Electrical Conductivity in Copper. *Science* **2004**, *304*, 422–426.
- (36) Proskuryakov, Y. Y.; Durose, K.; Taele, B. M.; Oelting, S. Impedance Spectroscopy of Unetched CdTe/CdS Solar Cells-Equivalent Circuit Analysis. *J. Appl. Phys.* **2007**, *102*, 024504.
- (37) Hegedus, S. S.; Shafarman, W. N. Thin-Film Solar Cells: Device Measurements and Analysis. *Prog. Photovoltaics* **2004**, *12*, 155–176.
- (38) Phillips, A. B.; Khanal, R. R.; Song, Z.; Zartman, R. M.; DeWitt, J. L.; Stone, J. M.; Roland, P. J.; Plotnikov, V. V.; Carter, C. W.; Stayancho, J. M.; Ellingson, R. J.; Compaan, A. D.; Heben, M. J. Wiring-up Carbon Single Wall Nanotubes to Polycrystalline Inorganic Semiconductor Thin Films: Low-Barrier, Copper-Free Back Contact to CdTe Solar Cells. *Nano Lett.* **2013**, *13*, 5224–5232.
- (39) Burst, J. M.; Duenow, J. N.; Albin, D. S.; Colegrove, E.; Reese, M. O.; Aguiar, J. A.; Jiang, C.-S.; Patel, M. K.; Al-Jassim, M. M.; Kuciauskas, D.; Swain, S.; Ablekim, T.; Lynn, K. G.; Metzger, W. K. CdTe Solar Cells with Open-Circuit Voltage Breaking the 1V Barrier. *Nature Energy* **2016**, *1*, 16015.
- (40) Proskuryakov, Y. Y.; Durose, K.; Taele, B. M.; Oelting, S. Impedance Spectroscopy of Unetched CdTe/CdS Solar Cells-Equivalent Circuit Analysis. *J. Appl. Phys.* **2007**, *102*, 024504.
- (41) Li, J. V.; Halverson, A. F.; Sulima, O. V.; Bansal, S.; Burst, J. M.; Barnes, T. M.; Gessert, T. A.; Levi, D. H. Theoretical Analysis of Effects of Deep Level, Back Contact, and Absorber Thickness on Capacitance-Voltage Profiling of CdTe Thin-Film Solar Cells. Sol. Energy Mater. Sol. Cells 2012, 100, 126–131.
- (42) Angeles-Ordóñez, G.; Regalado-Pérez, E.; Reyes-Banda, M. G.; Mathews, N. R.; Mathew, X. CdTe/CdS Solar Cell Junction Activation: Study using MgCl<sub>2</sub> as an Environment Friendly Substitute to Traditional CdCl<sub>2</sub>. Sol. Energy Mater. Sol. Cells **2017**, 160, 454–462
- (43) Gershon, T.; Lee, Y. S.; Antunez, P.; Mankad, R.; Singh, S.; Bishop, D.; Gunawan, O.; Hopstaken, M.; Haight, R. Photovoltaic Materials and Devices Based on the Alloyed Kesterite Absorber  $(Ag_xCu_{1-x})_2ZnSnSe_4$ . Adv. Energy Mater. 2016, 6, 1502468.
- (44) Li, J.; Wang, H.; Luo, M.; Tang, J.; Chen, C.; Liu, W.; Liu, F.; Sun, Y.; Han, J.; Zhang, Y. 10% Efficiency  $\text{Cu}_2\text{ZnSn}(S,\text{Se})_4$  Thin Film Solar Cells Fabricated by Magnetron Sputtering with Enlarged Depletion Region Width. *Sol. Energy Mater. Sol. Cells* **2016**, 149, 242–249.
- (45) Zeng, G. G.; Harrison, P.; Kidman, A.; Wu, J. Z.; Al-mebir, A.; Feng, L. Correlation of Microscopic Grain Evolution in Post-CdCl<sub>2</sub> Annealing and Performance of CdS/CdTe Thin-Film Solar Cells Fabricated Using Pulsed Laser Deposition. *Phys. Status Solidi A* **2016**, 213, 3231–3237.
- (46) Al-mebir, A. A.; Harrison, P.; Kadhim, A.; Zeng, G. G.; Wu, J. Z. Effect of In Situ Thermal Annealing on Structural, Optical, and Electrical Properties of CdS/CdTe Thin Film Solar Cells Fabricated by Pulsed Laser Deposition. *Adv. Condens. Matter Phys.* **2016**, 2016, 8068396.
- (47) Leite, M. S.; Abashin, M.; Lezec, H. J.; Gianfrancesco, A.; Talin, A. A.; Zhitenev, N. B. Nanoscale Imaging of Photocurrent and Efficiency in CdTe Solar Cells. *ACS Nano* **2014**, *8*, 11883–11890.
- (48) Tennyson, E. M.; Gong, C.; Leite, M. S. Imaging Energy Harvesting and Storage Systems at the Nanoscale. *ACS Energy Letters* **2017**, *2*, 2761–2777.